

DUPLICATE REFERENCE COPY

UCRL-JC-112577
PREPRINT

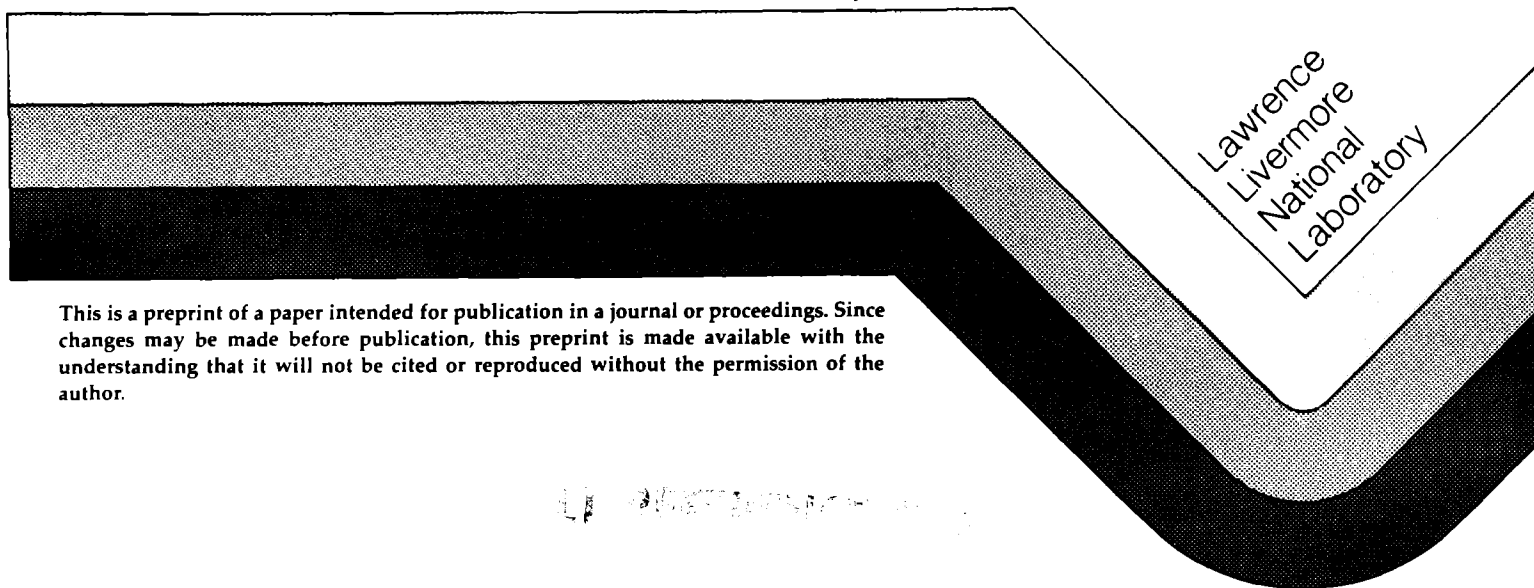


Gyrokinetic Simulations of Poloidal Velocity-Shear Effects on Ion-Temperature-Gradient Modes

Bruce I. Cohen
Timothy J. Williams
Andris M. Dimits
Jack A. Byers

THIS PAPER WAS PREPARED FOR SUBMITTAL TO
Physics of Fluids B

December 18, 1992



This is a preprint of a paper intended for publication in a journal or proceedings. Since changes may be made before publication, this preprint is made available with the understanding that it will not be cited or reproduced without the permission of the author.

DISCLAIMER

This document was prepared as an account of work sponsored by an agency of the United States Government. Neither the United States Government nor the University of California nor any of their employees, makes any warranty, express or implied, or assumes any legal liability or responsibility for the accuracy, completeness, or usefulness of any information, apparatus, product, or process disclosed, or represents that its use would not infringe privately owned rights. Reference herein to any specific commercial products, process, or service by trade name, trademark, manufacturer, or otherwise, does not necessarily constitute or imply its endorsement, recommendation, or favoring by the United States Government or the University of California. The views and opinions of authors expressed herein do not necessarily state or reflect those of the United States Government or the University of California, and shall not be used for advertising or product endorsement purposes.

Gyrokinetic Simulations of Poloidal Velocity- Shear Effects on Ion-Temperature-Gradient Modes

Bruce I. Cohen, Timothy J. Williams, Andris M. Dimits, and Jack A. Byers

Lawrence Livermore National Laboratory, University of California

P.O. Box 808, Livermore, California 94550

Abstract

Data from several current tokamak experiments indicate that the equilibrium poloidal velocity field can become strongly sheared accompanying the transition from L-mode to H-mode, i.e., improved, confinement and that fluctuation levels are reduced. Linear theory suggests that velocity shear can stabilize ion-temperature-gradient (ITG) modes when the frequency shift experienced by the mode due to the radial dependence of the Doppler shift is comparable to the growth rate. To confirm the predictions of linear theory and to explore nonlinear issues, e.g., self-generated shear flows, saturation amplitudes and the concomitant energy transport levels, two and three-dimensional gyrokinetic simulations of ITG modes have been performed. The simulations were done with and without magnetic shear in a slab configuration using the partially linearized (δf) algorithm to reduce statistical noise. The simulations confirm theoretical analyses of the stabilizing and destabilizing effects of imposed poloidal velocity fields. The ion energy transport levels at saturation follow the trends of the linear growth rates and the mixing length estimates. The gyrokinetic simulations are in qualitative agreement with the results of gyrofluid simulations, and exhibit saturation amplitudes and energy transport similar to those in gyrofluid simulations. These transport levels are generally lower than those typically reported in the laboratory experiments, much of which discrepancy is reduced when toroidal driving terms are included.

PACS numbers: 52.35.P, 52.35.R, 52.65

I. INTRODUCTION

Experiments on several large and small tokamaks¹⁻⁷ suggest a correlation between the onset of improved confinement (L-H transition) and the emergence of strong shear in the poloidal rotation just inside the edge of the plasma. Theoretical models for the development of shear in the poloidal velocity and its relation to improved confinement have been presented.⁸⁻¹⁰ Other theoretical papers have addressed the possible stabilizing effect that a strongly sheared poloidal velocity field might have on the drift-type modes that produce turbulent transport.¹¹⁻¹⁶ These analyses suggest that strong poloidal velocity shear causes improved confinement via linear stabilization of drift-type modes. Nonlinear fluid and gyrofluid simulations of ion-temperature-gradient (ITG) turbulence by Hamaguchi and Horton¹⁴ and by Waltz, et al.¹⁵ demonstrate velocity-shear stabilization. In contrast, Carreras, et al. have analysed a model that indicates that nonlinear effects defeat the linear stabilization effect of externally imposed poloidal velocity shear on the dissipative trapped electron mode for a velocity that varies linearly in space.¹⁷ However, Ref. 17 also points out that self-consistent nonlinearly generated flows should reduce turbulence levels.

This paper presents the first reported gyrokinetic simulation¹⁸ of the effects of strong poloidal velocity shear on ITG modes. Earlier gyrokinetic simulation studies of ITG modes did not examine the effects of velocity shear and were undertaken with a fully nonlinear gyrokinetic model in Refs. 19 and 20. We take an externally imposed $\mathbf{E} \times \mathbf{B}$ velocity field with either linear or parabolic spatial variation and also with a self-consistent model of flow, and follow the linear growth and nonlinear saturation of ITG modes. Electrons are modeled with a linear adiabatic fluid response.¹⁸ The ions are modeled as a nonlinear gyrokinetic species using the partially linearized (δf) algorithm to reduce statistical noise effects.^{21,22} Kotschenreuther has used a δf code to study ITG modes, but did not report any study addressing velocity shear effects.²² Our results generally concur with linear theory^{13,14} and the fluid simulations of ITG turbulence^{14,15} indicating that

strong poloidal velocity shear has a stabilizing influence on turbulence, improves confinement, and could be a contributing mechanism to the L-H transition.

The paper is organized as follows. In Sec. II the simulation model is described, and some convergence tests are presented. Simulation results for ITG modes are given in Sec. III. Externally imposed velocity shear with linear variation in x is found to be destabilizing for weak shear and eventually stabilizing when $V_0' L_s / c_s > 2$, independent of the sign of V_0' . Here $V_0' = dV_E/dx$, where V_E is the y -component of the imposed $\mathbf{E} \times \mathbf{B}$ drift velocity, L_s is the magnetic shear length, and c_s is the ion sound speed. When strong velocity shear is switched on while the ITG turbulence is growing, there is a strong stabilizing effect. Nonlinear effects do not appear to defeat the stabilizing effects of the velocity shear. This agrees with the gyrofluid simulation results of Waltz, et al.¹⁵ The effects of velocity shear with a parabolic spatial dependence are found to be weak for the parameters of our simulations. The inclusion of self-generated ion flows in the simulations leads to the emergence of strong self-generated shear flows that are stabilizing. Some discussion of the energy transport observed in our simulations is given in Sec. IV along with its scaling to experiments and a comparison to gyrofluid simulations. The peak energy transport rates observed in our simulations track γ/k^2 values using the wavenumber of the fastest growing mode and are similar in magnitude to the transport rates observed in gyrofluid simulations.¹⁵

II. Gyrokinetic Simulation Model

The electrostatic gyrokinetic particle simulation model has been described elsewhere in detail.¹⁸ Here we use a variant of that model in which the so-called parallel nonlinearity has been omitted to make a partially linearized or δf algorithm.^{21,22} By this we mean that where $(q/m)E_z \partial f / \partial v_z$ appears in the Vlasov equation, $\partial f / \partial v_z$ is computed analytically just from the unperturbed, Maxwellian distribution function. This allows one to represent only the perturbation of the distribution function from a Maxwellian with particles, and thus

reduce the statistical noise by a large factor because the perturbations considered are small. To implement this, the ions are advanced along their $\mathbf{E} \times \mathbf{B}$ trajectories and ballistically stream parallel to the magnetic field. The magnetic field is allowed to be sheared in the y - z plane, i.e., its y component has x dependence. The $\mathbf{E} \times \mathbf{B}$ drift is the gyroaveraged drift as approximated by a four-point average around the cyclotron orbit. The approximately gyroaveraged perturbed ion charge density is accumulated on a spatial grid, and the gyrokinetic Poisson equation is solved with the electron response modeled as adiabatic.¹⁹

Equilibrium density and temperature variations in x are modeled with a linearized, multi-scale treatment that leads to a source term for the δf particle weights.²¹ The $k_x=0$ components of the perturbed potential are suppressed. This multi-scale treatment is strictly valid only in the limit that the equilibrium scale lengths are long compared to the wavelengths of the waves simulated. Thus, we can only simulate legitimately a small subdomain of the plasma cross-section with this assumption invoked. The use of the partially linearized multi-scale model in conjunction with the δf approximation and the neglect of the parallel nonlinearity provides the additional advantage that there is an exact scaling of the model with respect to the scale lengths of the equilibrium density and temperature profile. The simulation results can be scaled to any strength of the equilibrium density or temperature gradient.²³

The adiabatic electron response model has a particular feature of interest. Nonlinear, self-generated flows in the ions can have important components with $k_y=0$ and $k_z=0$, i.e., the parallel wavenumber $k_{\parallel}=0$. This component of the electric potential (for $k_x \neq 0$) is retained in the simulation when we wish to include self-generated ion flows; otherwise, the $k_y=k_z=0$ Fourier components of the electric potential are suppressed. The linear electron response to the $k_y=k_z=0$ Fourier mode is zero, and the nonlinear adiabatic electron response is negligible in the δf regime. There could be a nonlinear, nonadiabatic electron response that could be significant in some cases, but it would require a wholly

different electron model. For $k_y \neq 0$ or $k_z \neq 0$, so that $k_{\parallel} \neq 0$, the usual linear adiabatic electron model is applicable.¹⁹

The simulation model had periodic boundary conditions in the y and z dimensions. In the x dimension, the simulation box was extended to twice its length ($2L_x$); and periodic boundary conditions were applied on the extended domain. Particles leaving the physical domain ($x=0$ and $x=L_x$) were reflected back into the domain, and the self-consistent electric potential was forced to have nulls in x at the boundaries of the physical domain. The charge density was reflected with odd symmetry at $x=L_x$. To model an imposed equilibrium $\mathbf{E} \times \mathbf{B}$ velocity field, an applied potential was added to the self-consistent potential before computing the total electric field. The applied potential had either parabolic or cubic variation in x so that the $\mathbf{E} \times \mathbf{B}$ velocity had either constant first or second spatial derivative. To be consistent with being periodic on the extended domain in x , the applied potential had a jump at $x=(3/2)L_x$; but no particles could get to this point.

With the boundary conditions described and no sources of particles and energy, nonlinear effects can relax density and temperature gradients or gradients of the ion distribution in velocity space as the simulation evolves. In consequence, these initial-value simulations do not give rise to steady-state turbulent transport. The plasma is initialized to be unstable to ITG modes. Following the exponential growth of unstable ITG modes, nonlinear effects emerge, and saturation is observed. The transport of thermal energy grows and saturates along with the electric field fluctuations; it then relaxes the source of free energy driving the instability, although the average temperature gradient across the system is not observed to relax very much for the parameters of our simulations and density-gradient relaxation does not occur. After the thermal transport saturates, it subsides to a much smaller amplitude because there are no real sources to maintain the necessary gradients in configuration and velocity spaces.

We have undertaken two and three-dimensional, sheared-slab, δf gyrokinetic simulations of ITG modes. We have tested our gyrokinetic codes by conducting

simulations of ITG modes using the same parameters as those whose results have been reported by Lee and Tang,¹⁹ and by comparing linear growth rates and mode frequencies observed in the simulations to those computed either with a linear dispersion code similar to the shooting code used by Staebler and Dominguez¹³ or with the integral-equation, linear-dispersion code developed by Linsker.²⁴ Because the Linsker code makes no expansion for small $k_x \rho_i$ (ρ_i is the Larmor radius of a thermal ion), it is more applicable than the shooting code. When we focussed attention on just the linear regime of instability and initialized the δf code at very small initial amplitudes with an ordered filling of phase space, we obtained excellent agreement between our simulation results and those of the Linsker code for the mode frequencies and growth rates. The shooting code generally gave less accurate estimates for the real part of the mode frequencies than for the growth rates when compared to our gyrokinetic results and to the results of the Linsker code: for the fundamental eigenmode the gyrokinetic and the Linsker codes exhibited real frequencies that were up to $\sim 50\%$ larger in magnitude than those of the shooting code for $0.4 \leq k_y \rho_i \leq 1.0$.

Two related computational issues received significant attention in the course of this effort: statistical resolution and spatial filtering. All particle simulations are subject to statistical resolution constraints. Even with the increased leverage of the δf algorithm, statistical requirements can be demanding. As spatial resolution is increased, one must increase the total number of particles in order to insure that there are adequate numbers of particles per relevant wavelength to resolve the charge density. Because finite differencing produces a significant distortion of the fundamental equations at the shortest wavelengths admitted by the simulation, almost all particle simulations resort to spatial filtering or smoothing at short wavelengths. If relatively fewer modes are retained in the simulation because the short wavelength modes are heavily attenuated, then fewer particles are required to resolve the charge density.

To establish confidence in our methods, we performed multiple simulations holding all physical and computational parameters fixed except for the number of particles per cell, which we increased from simulation to simulation until the physical results converged (Fig. 1). This was a demonstration that we had adequate statistical resolution to insure that the physical signal adequately exceeded the noise throughout the simulation. For our three-dimensional ITG δf simulations with $\exp(-k^6 a^6)$ filtering applied to the charge density in k -space, we found that using ≥ 30 particles per cell was adequate for $a = \rho_i$. The number of particles cited here is conservative. If one wishes to resolve merely the maximum electric field amplitudes and the cross-field thermal fluxes, and is somewhat indifferent to the values of these quantities in the relaxed state following saturation, then many fewer particles are required for statistical resolution (~ 5 - 10 particles per cell). We also varied the magnitude of the wavenumber for which smaller wavenumbers were relatively unattenuated and larger ones were significantly damped, and varied the power of ka appearing in the exponential smoothing factor (Fig. 2). In this manner we determined whether enough of the physically relevant wavenumber spectrum was being retained so that the physics results were not being distorted significantly by spatial filtering. We settled on a spatial filtering factor $\exp(-k^6 a^6)$ with $a_x = a_y = a_z \sim \rho_i$ to strongly attenuate short-wavelength modes $k\rho_i > 1$ and to leave the long wavelength modes $k\rho_i \leq 1$ unattenuated.

III. SIMULATIONS OF ITG MODES WITH VELOCITY SHEAR

In this section, we present the results of our gyrokinetic simulations of the effects of velocity shear on ITG turbulence. It is useful to consider the following simple heuristic arguments. The spread in local Doppler shifts in the mode frequency over the width Δx of the mode is approximately $k_y V_0' \Delta x$ for a linear velocity shear profile and $k_y V_0'' \Delta x^2 / 2$ for a parabolic profile with $V_0' = 0$ for a value of x halfway across the physical domain, where $B_y = 0$ in the magnetically sheared cases. When the spread in Doppler shifts becomes comparable to the mode growth rate, one expects significant modification of both the linear

growth rates and the saturated turbulence. For strongly unstable ITG modes, the growth rates of the most unstable modes are comparable to the parallel streaming frequency $k_{\parallel}c_s$, where the effective parallel wavenumber is $k_{\parallel} \sim k_y \Delta x / L_s$ in a magnetically sheared plasma. Equating the spread of Doppler shifts to the mode frequency, one obtains

$$V_0' L_s / c_s \sim 1 \quad (1)$$

for a linear variation in the $\mathbf{E} \times \mathbf{B}$ velocity profile and

$$V_0'' \rho_i L_s / c_s \sim 1 \quad (2)$$

for a parabolic $\mathbf{E} \times \mathbf{B}$ velocity profile and a linear mode width scaling as $\Delta x \sim \rho_i$.

Calculations of the linear stability of ITG modes in the presence of velocity shear^{13,14,25} agree qualitatively with Eqs.(1) and (2), and provide quantitative details. The linear theory of Staebler and Dominguez¹³ indicates that, for a linear velocity-shear profile and a specific choice of plasma parameters motivated by the shear layer in the DIII-D experiment, the effect of increasing velocity shear with an adiabatic electron response is to leave the linear growth rates essentially unchanged for weak velocity shear $V_0' L_s / c_s < 1$, then to decrease the linear growth rates steadily for more shear, and to stabilize the mode for $V_0' L_s / c_s > 2-3$. For a fully kinetic electron response, there is a weak destabilization of the mode as $V_0' L_s / c_s$ increases from zero to unity in value, after which the growth rate decreases and the mode is stabilized for slightly higher values of $V_0' L_s / c_s$ than in the case of adiabatic electrons. The Doppler shift causes the real part of the frequency to steadily decrease in magnitude with increasing $V_0' L_s / c_s$ until the mode frequency passes through zero. The eigenmode structure exhibits a shift off the mode rational surface where $k_{\parallel} = 0$, which increases with increasing velocity shear. The eigenmode equation is invariant under the transformation $x \rightarrow -x$ and $V_0' \rightarrow -V_0'$, so that the eigenvalues are insensitive to the sign of V_0' . Negative values of V_0'' are stabilizing, while $V_0'' > 0$ is weakly destabilizing until very large positive values of V_0'' ($V_0'' \rho_i L_s / c_s > 3$) render the mode stable. The real part of the frequency becomes less negative with increasing V_0'' .

A. Simulations with externally imposed shear flows

To investigate the effects of velocity shear on the ITG instability, we performed two and three-dimensional gyrokinetic simulations. Our parameter choices were motivated generally by those appropriate to the DIII-D shear layer,^{5,13} but are not intended to exactly match DIII-D. Our two-dimensional simulations had a sheared magnetic field given by $B_z=B_0$ and $B_y=B_0(x-x_0)/L_s$ with a single mode-rational surface bisecting the x-y domain at $x_0=16\rho_i$. With no magnetic shear, the magnetic field was tilted so that $B_y=\theta B_0$ and only modes with $k_z=0$ were kept. We performed two-dimensional simulations with $\eta_i=L_n/L_T=\infty$, $L_s/L_T=33.3$, $\tau=T_e/T_i=1$, $L_x=L_y=32\rho_i$, and a series of $V_0 L_s/c_s$ values, where $T_{e,i}$ are the electron and ion temperatures, L_n and L_T are the density and temperature gradient scale lengths. When linear growth rates were compared to the predictions of a shooting code, the results disagreed by 20-50% for $k_y\rho_i=0.4$. For a set of simulations with $V_0 L_s/c_s=0, 1, 2$, and 4, we observed some weak destabilization when we increased the relative velocity shear from zero to $V_0 L_s/c_s=1$, little change going to 2, and a strongly stabilizing effect for a value of 4. The normalized averaged ion thermal flux in x from these simulations is plotted as a function of $V_0 L_s/c_s$ in Fig. 3.

The magnetic shear in the velocity shear layer may be quite weak relative to the plasma inhomogeneities near the edge of the tokamak. What effect does velocity shear have on the ITG instability when there is no magnetic shear? With $\eta_i=2$, $\tau=1/2$, $\theta L_T/\rho_s=0.075$, $\theta\ll 1$, $L_x=L_y=64\rho_s$, we compare simulation results for the spatially averaged normalized ion thermal flux with $V_0 L_T/c_s=0$ and 0.02 in Fig. 4. We observe that strong velocity shear is again stabilizing even when there is no magnetic shear, an observation previously made by Hamaguchi and Horton.¹⁴

Our magnetically sheared slab simulations in three dimensions have many mode rational surfaces. The mode rational surfaces become more closely spaced for the modes with larger wavenumbers k_y , and the nonlinear interaction between neighboring modes can occur more readily. This circumstance may alter the effects of velocity shear on drift-type

instabilities.¹⁷ In our three-dimensional sheared-slab simulations we used parameters $L_x=L_y=32\rho_i$, $L_z=1600\rho_i$, with the grid spacing in z elongated by a factor of 100 over the x - y grid spacing, $\eta_i=\infty$, $L_S/L_T=30$, $L_S/\rho_i=1000$, $\tau=1$, and 600,000 particle ions. Phase space was loaded with ions relatively uniformly, and the initial weights of the δf particles were set at a low level of 10^{-5} to allow the observation of a few decades of unstable growth in the linear phase.

We conducted three-dimensional simulations in which $V_0 L_S/c_s=0, 1, 2, 3$, and -3 . Self-generated ion flows were suppressed by discarding the $k_y=k_z=0$ Fourier modes of the electric potential. The peak values of the effective potential energy (the sum of the field, ion polarization, and adiabatic electron kinetic energies) and the normalized, spatially averaged ion thermal flux in x increased significantly going from the $V_0 L_S/c_s=0$ to 1 (Fig. 5). The linear theory of ITG instability due Wang et al. showed that weak velocity shear can be destabilizing.²⁵ This does not contradict the results of Ref. 13, which found no significant destabilization, because the numerical calculations in Refs. 13 and 25 were performed with different physical parameters. We have confirmed the numerical results of Refs. 13 and have obtained results qualitatively similar to Ref. 25 with a shooting code that solves the linear dispersion relation. The mode frequencies in our simulations decreased in magnitude on account of the $E \times B$ Doppler shift as V_0 was increased. The wavenumber spectra had a relatively broad peak at wavenumbers $|k_y \rho_i| \leq 0.6$ and $|k_z \rho_i| \leq 0.004$, and there was no obvious evidence of steady coherent structures forming at saturation. With $V_0 L_S/c_s=2$, the Doppler shift increased to the point that the mode frequencies of the lowest principal modes changed sign relative to the $V_0 L_S/c_s=0$ case; and the total electrostatic energy and the thermal flux slightly decreased from their levels for $V_0 L_S/c_s=1$ (Fig. 6). For $V_0 L_S/c_s=3$, there was significant stabilization of the ITG modes: the observed growth rates, the total electrostatic energy, and the thermal flux were much reduced over the $V_0 L_S/c_s=0$ case. The mode frequencies were Doppler shifted to opposite signs relative to the $V_0=0$ case. With $V_0 L_S/c_s=-3$, the detailed histories of the fluctuation spectra and

transport differed very little from those in the $V_0 \Gamma_s/c_s=3$ simulation. In Figure 7 we show the time history of the spatially averaged ion thermal flux in x for a simulation in which we switched $V_0 \Gamma_s/c_s$ from 0 to 3 half way through the simulation. This result should be compared to the time history shown in Fig. 1b for the same parameters but with no imposed velocity shear throughout. Switching on strong velocity shear moderated the further growth of the ITG modes and was significantly stabilizing. A similar result was reported in a gyrofluid simulation reported in Ref. 15.

We did two simulations with V_0'' finite and $V_0'=0$ at the midplane of the simulation in x where $B_y=0$. Results are shown in Figure 8. With $V_0'' \rho_i L_s/c_s = 1.8$, we observed no significant shift of the ITG mode frequencies from the case of no velocity shear and a small enhancement of the total electrostatic energy and ion thermal flux. With $V_0'' \rho_i L_s/c_s = -1.8$, there was again no significant shift of the real part of the mode frequencies, but there was a small decrease in the growth rates, while the electrostatic energy and the ion thermal flux were not much changed from the corresponding values in the case with no velocity shear. The weakness of the effects and the dependence on the sign of V_0'' of the stabilizing and destabilizing effects agree qualitatively with the linear theory of Staebler and Dominguez.¹³

B. Simulations with self-generated shear flows

In order to obtain evidence on the role of self-generated sheared ion flows in the simulations, we had to modify the simulation model. The Fourier modes of the electric potential that are associated with self-generated nonlinear $\mathbf{E} \times \mathbf{B}$ flows in the y direction, i.e., modes with $k_x \neq 0$ and $k_y = k_z = 0$, were retained. In two dimensions $k_z = 0$, so the condition is just $k_y = 0$. For these modes, we take the electron density response to be zero. This amounts to neglecting the radial particle transport of the electrons, because parallel acceleration and parallel streaming cannot produce a finite flux-surface-averaged particle density perturbation. Also, $E_{\parallel} = 0$ for these modes; so there is no linear Boltzmann response. Nonlinear and nonadiabatic electron effects are omitted by this model. In three-dimensional simulations with self-generated ion flows, the growth of a substantial amount

of self-generated sheared ion flow accompanied the growth of the ITG modes; and there was a net reduction in the thermal diffusivity by a factor of ~ 3 in the peak value compared to the case with no imposed or self-generated shear flow (see Figs. 1b and 9). From the $e\phi/T_e$ vs. x profile after saturation (Fig. 9), which is dominated by the $k_y=k_z=0$ mode, we deduce that the self-generated flow became strongly sheared: $|V_0 \nabla L_S/c_s| \leq O(5)$ and $|V_0 \nabla \rho_S L_S/c_s| \leq O(1)$ depending on the x position. The magnitude of the peak self-generated shear flow exceeded the values of imposed shear flow that we found to be strongly stabilizing.

In order to investigate the shear-flow generation mechanism more easily and in more detail, we performed two-dimensional simulations with periodic radial boundary conditions and no magnetic shear. This choice avoids the effects of separated phase-space resonances, to be discussed later, and prevents saturation by quasilinear flattening of the temperature profile. A baseline simulation was made with the $k_y=0$ mode of the electric potential retained and with the following parameter values: 2.6×10^5 particles, $\eta_i = \infty$, $L_x=L_y=32\rho_i$, $\theta L_T/\rho_i=0.075$, $a_x=a_y=1.7$. Additional simulations were performed in which the parameter values and the physics contained in the model were altered from those of the baseline. For the baseline, the ion thermal diffusivity rose to a peak value of $\hat{\chi}_i = \chi_i/(c_s \rho_S^2/L_T) \sim 0.6$ in gyro-reduced Bohm units, before dropping to zero. The drop coincided with the generation of strong $\mathbf{E} \times \mathbf{B}$ flows, mainly in the first and second k_x modes with peak values in space of $V_0 \nabla L_T/c_s \sim 0.7$. This can be compared with the value of $V_0 \nabla L_T/c_s \sim 0.1$ that was sufficient to stabilize the modes when a linear $V_0(x)$ was imposed. A check of convergence of the simulation results made with 4.9×10^5 particles gave quite similar results. In another simulation with the same parameter values, but with the $k_y=0$ mode of the electric potential controlling the self-generated flow set to zero, the normalized diffusivity peaked at $\hat{\chi}_i \sim 2.6$ and dropped to a finite steady value $\hat{\chi}_i \sim 1.6$. These simulations again confirm that the self-generated flow greatly reduces the peak thermal flux and leads to a similar conclusion for the post-saturation flux.

Because the $k_y=0$ mode in two dimensions and the $k_y=k_z=0$ mode in three dimensions are linearly stable, their generation is a nonlinear process. The nonlinearities can be grouped into two categories:²⁶ the polarization nonlinearities and the finite-Larmor-radius (FLR) nonlinearities (in the absence of FLR, the $\mathbf{E}\times\mathbf{B}$ advection nonlinearity is absent in a quasineutral plasma in which the electrons are adiabatic). The latter are distinguished by the fact that they vanish in the limit $\tau=T_e/T_i\rightarrow 0$. In our simulations $\tau=1$, and both nonlinearities were active.

In order to understand which of these nonlinearities is important for the flow-generation process, two simulation runs were made with FLR terms suppressed. In the first of these, the Larmor radii of all of the simulation ions were set to zero, while the polarization density term in the gyrokinetic Poisson equation was retained. This procedure removes all of the linear and nonlinear FLR terms. The parameter values were otherwise the same as for the baseline simulation. The resulting peak flux was reduced to $\hat{\chi}_i\sim 0.2$. Again strong sheared $\mathbf{E}\times\mathbf{B}$ flows were generated, and the flux dropped to zero. The peak values of the flow shear were $V_0 L_T/c_s\sim 0.6$. The second simulation was made with the perpendicular temperature gradient set to zero, but with standard finite ion Larmor radii. This eliminated the FLR terms that involve fluctuations of the perpendicular temperature. (In the collisionless limit, in which the pressure is anisotropic, the only temperature involved in the FLR terms is the perpendicular temperature.) The total peak flux was $\hat{\chi}_i\sim 0.14$, only slightly lower than for the previous case, even though in this case the thermal flux is entirely the flux of the parallel temperature. The modal content and the values of the shear in the self-generated flow were almost identical to those of the first case.

We conclude that although the FLR nonlinearities may play a role in the details of the evolution, they are not essential to the flow generation process. The final states in all of the cases in which the self-generated flow was kept were similar. The differences in the peak flux values could be caused by differences in linear growth rates as well as by nonlinear effects. Unfortunately, the removal of the polarization nonlinearity is much more

difficult in a gyrokinetic code, so we have not determined if the FLR nonlinearities alone can result in self-generated flows. We can speculate that they should be able to since for a quasineutral plasma with adiabatic electrons, in the small ion-Larmor-radius limit, the FLR nonlinear term associated with the ion density fluctuations is identical in form to the polarization nonlinearity.²⁶

We also conclude that externally imposed stabilizing shear flow was *not* rendered irrelevant by nonlinear effects in our simulations with the self-generated $k_y=k_z=0$ component of the shear flow suppressed in contrast to the findings of Ref. 17 for a simplified fluid model of long wavelength dissipative drift waves. However, the reduction in turbulence levels observed in our simulations including the self-generated shear flow qualitatively agrees with the prediction of Ref. 17.

IV. DISCUSSION

The simulation results presented here agree qualitatively and, at least, semi-quantitatively with the linear stability calculations of Staebler and Dominguez,¹³ and Hamaguchi and Horton,¹⁴ and with the nonlinear fluid calculations of Waltz et al.¹⁵ and Hamaguchi and Horton.¹⁴ Increasing linear velocity shear is stabilizing, and the linear theory gives fairly good guidance as to when stabilization is nearly complete. The stabilization does not depend on the sign of V_0' , but may depend weakly on the sign of V_0'' . We agree with the earlier fluid simulations of Hamaguchi and Horton¹⁴ that velocity-shear stabilization of ITG modes is effective even when there is no magnetic shear. We see no evidence of nonlinear destabilization of ITG modes defeating linear velocity-shear stabilization. As in the gyrofluid simulations of Waltz et al.,¹⁵ when strong velocity shear was switched on in the middle of a simulation which was unstable to ITG modes, the amplitude of the turbulent fluctuations decreased and the cross-field ion thermal transport decreased dramatically. When self-generated flows are admitted in the simulations, they appear to have an important stabilizing effect.

To put these gyrokinetic simulation results into a context where they may be more easily compared to other calculations and to experimental values, we consider the intrinsic scaling of this model. From a straightforward scaling theory,²³ one can deduce that the ion energy diffusivity χ_i for ITG turbulence scales as²⁷

$$\chi_i = (c_s \rho_s^2 / L_n) f((1+\eta_i)T_i/T_e, L_n/L_s) , \quad (3)$$

where f is some additional function of the given dimensionless factors that cannot be determined from the scaling arguments. This scaling is exact for the multi-scale δf gyrokinetic model. One recognizes the gyro-reduced Bohm scaling in the leading coefficient on the right side of Eq.(3). The x -directed, normalized ion energy flux Q_x in our simulations is related to the true ion thermal flux by $Q_x = q_x / (c_s T_i)$. The ion energy diffusivity is related to the divergence of the heat flux by $\chi_i dT_i/dx = q_x$, from which follows that $\chi_i \sim L_T q_x / T_i \sim c_s L_T Q_x$ and

$$\chi_i = (L_T L_n / \rho_s^2) Q_x (c_s \rho_s^2 / L_n) . \quad (4)$$

Thus, $\hat{\chi}_i = (L_T L_n / \rho_s^2) Q_x$ is the ion diffusivity in gyro-reduced Bohm units and allows us to translate the simulation data into a form useful for comparisons. In the limit $L_n = \infty$ and $L_T \neq 0$ that corresponds to most of the ITG simulations described here, the L_n factors that appear in Eqs.(3) and (4) should be replaced by $L_T T_e / T_i$.

Here we compare our simulation results for $\hat{\chi}_i$ to the results of other simulations and to those inferred from experiments. These comparisons collect data from several sources in which the physical parameters, the numerical models, the boundary conditions, and parameters vary. Furthermore, caution should be exercised in making comparisons between the peak transport rates in our initial-value simulations and the steady-state transport rates measured in some other simulation models and inferred from experimental data. To the extent that the initial conditions in our simulations, both the temperature and density gradients and the ion distribution function, are representative of the steady-state plasmas that we are trying to model and given that the peak transport rates in our

simulations occur before there has been much relaxation of the initial conditions, then the comparisons are physically meaningful.

Our two-dimensional, magnetically sheared simulations exhibited peak values of $\hat{\chi}_i \leq 0.02$ (χ_i scaled to $c_s \rho_s^2 / L_T$). Our three-dimensional simulations yielded $\hat{\chi}_i \sim 0.1$ peak values. Lee and Tang¹⁹ reported peak values $\hat{\chi}_i \sim 0.1$ and asymptotic values $\hat{\chi}_i \sim O(0.01)$ for $\eta_i = 4$, a relatively coarse 16×16 grid, 64 particles per cell, a tilted unshaped magnetic field, a small system in which coherent nonlinear structures were observed, and fully nonlinear simulation (no δf approximation and retention of the parallel nonlinearity). Our two-dimensional simulations with no magnetic shear had larger system sizes and were more turbulent than those in Ref. 19. We used $\eta_i = \infty$ and a more unstable value of $\theta L_T / \rho_s$ than those used in Ref. 19. The resulting peak and asymptotic thermal diffusivities, in the absence of self-generated flows, were of order $\hat{\chi}_i \sim 2$. When self-generated flows were included, the peak values were lower, although still much higher than those reported elsewhere, while at late time the flux dropped to zero. In our tests of convergence with respect to particle number, we found that for particle numbers less than the converged values, the peak flux was always lower than the converged value, and a finite time-asymptotic flux was present.

In three-dimensional, fully nonlinear gyrokinetic sheared-slab simulations of a larger system with better grid resolution, but only 4 particles per cell, Sydora et al.²⁰ obtained spatially averaged values $\hat{\chi}_i \leq 0.01$ for $\eta_i = 4$ and peak values $\hat{\chi}_i \sim 0.1$ when averaging over 10% of the volume in which the principal mode rational surfaces were located. Our own experience with fully nonlinear gyrokinetic simulations in this parameter regime makes us question whether 4 particles per cell was sufficient to give adequate statistical convergence unless very strong spatial filtering was used. Even with δf methods, we found that we needed more than 5 particles per cell to insure adequate statistical resolution in our three-dimensional simulations. Kotschenreuther's three-

dimensional, sheared-slab, gyrokinetic δf simulations of ITG modes with particle statistics and grid resolution similar to ours and no applied velocity shear yielded $\hat{\chi}_i \sim 0.05-0.1$.²⁸

The three-dimensional sheared-slab gyrofluid simulations of velocity-shear stabilization of ITG modes undertaken by Waltz et al.¹⁵ exhibited values of $\hat{\chi}_i \sim 0.02-0.05$ at saturation for $\eta_i=2$ and $L_s/L_n=6-12$. The three-dimensional fluid simulations of Hamaguchi and Horton¹⁴ using a simpler fluid model surveyed a range of velocity and magnetic shear parameters, and yielded $\hat{\chi}_i \sim 0.1-0.5$. Thus, the slab gyrofluid simulation results for $\hat{\chi}_i$ are similar to those obtained in δf gyrokinetic simulations; and both are lower than those produced by simpler fluid models. However, careful comparisons with identical physical parameter sets and spatial numerical resolution have not been undertaken yet. Recent simulations by Dorland, Hammett, and Hahm with a gyrofluid code including a more detailed treatment of linear and nonlinear finite-ion-gyroradius effects indicate closer agreement with gyrokinetic calculations.²⁹

Typical experimental values of $\hat{\chi}_i$ in the shear layer of DIII-D are $\hat{\chi}_i \sim 1-10$;³⁰ and $\hat{\chi}_i \sim 0.1-2.0$ increasing with minor radius has been reported in the core of TFTR.³¹ One important physical ingredient, which has been omitted in all of the aforementioned numerical calculations and whose addition significantly increases the level of turbulence and the concomitant transport, is toroidicity.^{28,32} The additional driving force for instability contributed by toroidal curvature was shown to increase the transport by approximately a factor of ten in Kotschenreuther's three-dimensional gyrokinetic simulations of ITG turbulence so that $\hat{\chi}_i \sim 0.5-1.0$ were obtained.²⁸ By just including the gradient and curvature-B ion drift associated with toroidicity in our three-dimensional gyrokinetic simulation, $V_d = -(v_{\parallel}^2 + v_{\perp}^2/2)\hat{y}/R\Omega$, which gives a local model of the toroidal driving terms with no poloidal dependence, we observed a peak value of $\hat{\chi}_i \sim 0.6-0.8$ for a simulation with $\eta_i = \infty$, $L_s/L_T = 30$, $L_s/\rho_i = 1000$, no velocity shear, and $L_T/R = 0.1$ (R is the radius of curvature). With $V_0 L_s/c_s = 3$ and otherwise the same parameters, the peak value of the thermal diffusivity was $\hat{\chi}_i \sim 0.34$; and with $V_0 L_s/c_s = 5$ the peak diffusivity decreased

to $\chi_i \sim 0.0006$. In these simulations, the $k_y = k_z = 0$ Fourier component of the self-generated flow was suppressed.

In an effort to understand the relaxation mechanism at work in our simulations, we have calculated the time-integrated ion thermal transport. By integrating the ion thermal flux with respect to time through the peak of the time history to the first minimum in Q_x that approaches the asymptotic relaxed value, we obtain a number that can be compared to the amount of thermal energy transported through a distance that is required to flatten the global temperature gradient, $\sim (1/2L_T) (L_x/2)^2 T_i$. We observed relatively little variation in the time-integrated thermal transport for all of our three-dimensional sheared slab simulations, including the simulations with toroidal drive (except for the simulation with $V_0 L_S/c_s = 5$ which could be argued as being linearly stable). The effect of velocity shear when stabilizing was to reduce the magnitude of the peak in Q_x and to broaden it in time keeping the area approximately constant (to within $\pm 25\%$). Overall the time-integrated thermal flux accounted for a relaxation of approximately 30% of the ion temperature gradient. Evidently the velocity shear influenced the thermal transport *rate* but did not affect the amount of free energy that had to be relaxed.

If only the resonant ions need to relax their contributions to the temperature gradient, then much less than the entire ion temperature gradient needs to flatten. To make a semi-analytical calculation of this tractable, we have made several simplifying assumptions. We have assumed that the modes extend over a distance $\Delta \sim 8\rho_s$ on each side of each mode rational surface in the x direction based on numerical solutions of the linear eigenvalue problem and that both the real and imaginary parts of the mode frequencies divided by k_y are independent of k_y . For a given value of v_{\parallel} the range in x over which a particular mode is resonant is calculated from the condition $|\omega - k_{\parallel} v_{\parallel}| \leq \omega_{E \times B} \sim \text{Im}\omega$ subject to the upper bound determined by the mode width Δ , where $k_{\parallel} = k_y(x - x_r)/L_S$, x_r is the location of a particular mode rational surface, and $\omega_{E \times B} \sim ck_x k_y \phi/B$ is the $E \times B$ trapping frequency. The intervals are defined by the values of k_y and k_z for all unstable modes. The local

flattening of the temperature gradient is accomplished with a divergence in the heat flux as constrained by $\partial T/\partial t + \partial Q/\partial x=0$, from which follows

$$(1/V)\int Q dx dt = (1/V)\int dx x \Delta T \quad (5)$$

with an integration by parts and the assumption that $Q=0$ at the x boundaries. Here V is the volume. The quantity $\Delta T/V$ is deduced from calculating the amount of energy needed to flatten the local temperature gradient over a distance x_c to x , i.e., $\Delta T/V = -(1/2)\int dv m v^2 (x-x_c) dF_M/dx$, where $dF_M/dx = -[\eta_i^{-1} + (v^2/2v_i^2) - 3/2]F_M/L_T$ and x_c is the center of each spatial interval; and the resonant intervals are summed over if they do not overlap. If intervals overlap in x for particular values of v_{\parallel} , then the integration in x extends over the union of the overlapping intervals. The resonant intervals in the (x, v_{\parallel}) plane are shown in Fig. 10 for parameters that are representative of our simulations. Expressions for $\Delta T_{\parallel}/V$ and $\Delta T_{\perp}/V$ can be obtained readily. Because dF_M/dx changes sign for $v^2/2v_i^2 < (3/2) - \eta_i^{-1}$ and there is more overlap of the resonant intervals at low energies (small v_{\parallel} in Fig. 10), there are partially cancelling contributions to the integrand on the right side of Eq.(5). For the model calculations we performed, the expressions for $\Delta T_{\parallel}/V$, $\Delta T_{\perp}/V$, and the total $\Delta T/V$ were positive. The conclusion was that the predicted thermal flux associated with resonant flattening was always much smaller than that required to flatten the overall temperature gradient.

Because of the simplifying assumptions, we cannot expect quantitative agreement of the relaxation model with the simulations. Depending on the detailed choice of parameters and the assumptions, the predicted integrated thermal flux spanned an order of magnitude 0.5-5% of that required to flatten the entire temperature gradient while the observations in the simulations were ~30%. Some of the discrepancy is due to the fact that ions that are considered nonresonant and non-diffusive in our model do diffuse in the simulations. Both the cross-field fluxes of parallel and perpendicular thermal energy predicted by the model calculation and observed in the simulations were positive. The relaxation mechanism outlined here is relatively insensitive to velocity shear as long as the

ITG instability is well above threshold, which is consistent with the observation that the time-integrated thermal flux was relatively insensitive to velocity shear. When we repeated the three-dimensional simulation with $V_0' = 0$ and doubled the box length in the z direction so as to double the density of mode rational surfaces, the electric field energy at saturation changed very little but the peak thermal transport rate was $\sim 50\%$ bigger and the time-integrated thermal transport was almost double its previous value. While we cannot extract a simple scaling with the density of mode rational surfaces from our relaxation arguments, the model certainly predicts that the integrated thermal transport and, hence, the temperature-profile relaxation should increase with increasing density of mode rational surfaces. Thus, there are several pieces of evidence to support the qualitative accuracy of the resonant flattening relaxation model.

A final interesting observation concerning our simulations is shown in Fig. 11, where we have plotted the measured values of $\hat{\chi}_i$ and γ/k^2 normalized to gyro-reduced Bohm transport $c_s \rho_s^2 / L_T$ as functions of $V_0' L_s / c_s$ and $V_0 L_s / c_s$ for simulations with the $k_y = k_z = 0$ Fourier component of the self-generated flow suppressed. For γ and k , we have used the observed growth rate and wavenumber of the mode of the fastest growing mode. We note that the scaling of $\hat{\chi}_i$ tracks the γ/k^2 formula. The agreement with the γ/k^2 estimate is interesting but not conclusively established by our data set. We do not have sufficient mode resolution to address questions regarding the wavenumber dependence of the γ/k^2 estimate. We emphasize that the peak of the mode spectrum usually occurs at longer wavelengths in the gyrokinetic simulations than does the maximum linear growth rate.

Comparisons of the different calculations of the level of turbulent fluctuations and transport at saturation given by gyrokinetic and fluid simulations continue. As the gyrofluid models continue to mature and more powerful computers enable gyrokinetic simulations with improved statistical and spatial resolution, the differences between the results of gyrofluid and gyrokinetic simulations are decreasing. With the inclusion of

toroidal effects the simulation results from both models are corresponding more closely to experiments in many respects.

ACKNOWLEDGMENTS

We are particularly grateful to N. Mattor for providing a shooting code, helping with calculations, valuable suggestions, and a careful reading of the manuscript. We are also grateful to L. LoDestro, G. Hammett, R. Dominguez, and R. Waltz for their assistance and encouragement in this effort. We thank J. Reynders and the Theory Group at the Princeton Plasma Physics Laboratory for making the Linsker code available. We also thank R. Sydora and W. Lee who furnished our original nonlinear gyrokinetic codes.

The simulation efforts addressing the study of turbulent transport and anomalous confinement in tokamaks, and the comparison of gyrokinetic and fluid simulation results reported here are part of a multi-institutional collaboration whose aim is to create a numerical tokamak. This research contributes to the Numerical Tokamak Project, which is an activity supported jointly by the Department of Energy's Office of Fusion Energy and the Office of Scientific Computing as part of the High Performance Computing and Communications Program. This work was performed for the U.S. Department of Energy under Contract W-7405-ENG-48 at the Lawrence Livermore National Laboratory.

REFERENCES

- ¹C. P. Ritz, R. D. Bengston, S. J. Levinson, and E. J. Powers, *Phys. Fluids* **27**, 2956 (1984).
- ²S. J. Zweben, *Phys. Fluids* **28**, 974 (1985).
- ³R. J. Taylor, M. L. Brown, B. D. Fried, H. Grote, J. R. Liberati, G. J. Morales, P. Pribyl, D. Darrow, and M. Ono, *Phys. Rev. Lett.* **63**, 2365 (1989).
- ⁴R. R. Weynants and R. J. Taylor, *Nucl. Fusion* **30**, 945 (1990).

- ⁵R. J. Groebner, K. H. Burrell, and R. P. Seraydarian, Phys. Rev. Lett. **64**, 3015 (1990).
- ⁶K. Ida, S. Hidekuma, Y. Miura, T. Fujita, M. Mori, K. Hoshino, N. Susuki, and T. Yamauchi, Phys. Rev. Lett. **65**, 1364 (1990).
- ⁷K. Ida, S. Hidekuma, M. Kojima, Y. Miura, S. Tsuji, K. Hoshino, M. Mori, N. Suzuki, T. Yamauchi, and the JFT-2M Group, Phys. Fluids B **4**, 2552 (1992).
- ⁸S.-I. Itoh and K. Itoh, Phys. Rev. Lett. **60**, 2276 (1988); S. -I. Itoh and K. Itoh, Nucl. Fusion **29**, 1031 (1989).
- ⁹K. C. Shaing and E. C. Crume, Jr., Phys. Rev. Lett. **63**, 2369 (1989); K. C. Shaing, E. C. Crume, Jr., and W. A. Houlberg, Phys. Fluids B **2**, 1492 (1990).
- ¹⁰A.B. Hassam, T. M. Antonsen, Jr., J. F. Drake, and C. S. Liu, Phys. Rev. Lett. **66**, 309 (1991).
- ¹¹H. Biglari, P. H. Diamond, and P. W. Terry, Phys. Fluids B **2**, 1(1990).
- ¹²Y. B. Kim, P. H. Diamond, and R. J. Groebner, Phys. Fluids B **3**, 2050 (1991).
- ¹³G. M. Staebler and R. R. Dominguez, Nucl. Fusion **31**, 1891 (1991).
- ¹⁴S. Hamaguchi and W. Horton, Phys. Fluids B **4**, 319 (1992).
- ¹⁵R. E. Waltz, G. D. Kerbel, G. W. Hammett, and R. R. Dominguez, Bull. Amer. Phys. Soc. **36**, 2279 (1991).
- ¹⁶F. L. Waelbroeck, T. M. Antonsen, Jr., P. N. Guzdar, and A. B. Hassam, Phys. Fluids B **4**, 2441 (1992).
- ¹⁷B. A. Carreras, K. Sidikman, P. H. Diamond, P. W. Terry, and L. Garcia, Phys. Fluids B **4**, 3115 (1992).
- ¹⁸W. W. Lee, J. Comput. Phys. **72**, 243 (1987).
- ¹⁹W. W. Lee and W. M. Tang, Phys. Fluids **31**, 612 (1988).
- ²⁰R. D. Sydora, T. S. Hahm, W. W. Lee, and J. M. Dawson, Phys. Rev. Lett. **64**, 2015 (1990).

- ²¹A. M. Dimits and W. W. Lee, "Partially Linearized Algorithms in Gyrokinetic Particle Simulation," Princeton University PPPL-2718 (October, 1990), accepted for publication in *J. Comput. Phys.*
- ²²M. Kotschenreuther, "Particle Simulations with Greatly Reduced Noise," in *Proceedings of the 14th International Conference on Numerical Simulation of Plasmas* (Annapolis, MD, 1991).
- ²³J. W. Connor and J. B. Taylor, *Nucl. Fusion* **17**, 1047 (1977); J. W. Connor, *Nucl. Fusion* **26**, 193(1986).
- ²⁴R. Linsker, *Phys. Fluids* **24**, 1485 (1981).
- ²⁵X.-H. Wang, P. H. Diamond, and M. N. Rosenbluth, *Phys. Fluids B* **4**, 2402 (1992).
- ²⁶W. Horton, R. D. Estes, and D. Biskamp, *Plasma Phys.* **22**, 663 (1980).
- ²⁷L. L. LoDestro, B. I. Cohen, R. H. Cohen, A. M. Dimits, Y. Matsuda, W. M. Nevins, W. A. Newcomb, T. J. Williams, A. E. Koniges, W. P. Dannevik, J. A. Crotinger, A. K. Amala, R. D. Sydora, J. M. Dawson, S. Ma, V. K. Decyk, W. W. Lee, T. S. Hahm, H. Naitou, and T. Kamimura, "Comparisons of Simulations and Theory of Low-Frequency Plasma Turbulence," in *Proceedings of the Thirteenth International Conference on Plasma Physics and Controlled Nuclear Fusion Research*, Washington, D.C., 1990, (IAEA, Vienna, 1991), Vol. 2, p. 31.
- ²⁸M. Kotschenreuther, H. L. Berk, M. Lebrun, J. Q. Dong, W. Horton, J.-Y. Kim, D. W. Ross, T. Tajima, P. M. Valanu, H. V. Wong, W. Miner, D. C. Barnes, J. U. Brackbill, K. M. Ling, R. A. Nebel, W. D. Nystrom, J. A. Byers, B. I. Cohen, R. H. Cohen, A. M. Dimits, L. L. LoDestro, N. Mattor, G. R. Smith, T. J. Williams, G. D. Kerbel, J. M. Dawson, R. D. Sydora, B. A. Carreras, N. Dominguez, C. L. Hedrick, J.-N. Leboeuf, H. Naitou, and T. Kamimura, "Simulations for Confinement in Near-Fusion Experiments," in *Proceedings of the Thirteenth International Conference on Plasma Physics and Controlled Nuclear Fusion Research*, Wurzburg, Ger., 1992, (IAEA, Vienna, 1993), to be published.

²⁹W. Dorland, G. W. Hammett, L. Chen, W. Park, S. C. Cowley, S. Hamguchi, and W. Horton, in *Proceedings of the International Sherwood Fusion Theory Conference* (Santa Fe, NM, 1992), 3C2.

³⁰R. J. Groebner, W. Pfeiffer, F. P. Blau, K. H. Burrell, E. S. Fairbanks, R. P. Seraydarian, and H. St. John, *Nucl. Fusion* **26**, 543 (1986).

³¹S. D. Scott, et al., *Phys. Fluids B* **2**, 1300 (1990).

³²G. M. Staebler, R. E. Waltz, M. Beer, et al., "Profile Characteristics of H-mode Bifurcation Models and Turbulence Simulations with Gyro-Landau Fluid Models in Slab and Toroidal Geometry," in *Proceedings of the Thirteenth International Conference on Plasma Physics and Controlled Nuclear Fusion Research*, Wurzburg, Ger., 1992, (IAEA, Vienna, 1993), to be published.

Figure Captions

Figure 1. Normalized ion thermal flux in x expressed in terms of the ion thermal diffusivity (see Eq.(4)) as a function of time for simulations with (a) 1×10^5 , (b) 2×10^5 , and (c) 4×10^5 particle ions, and a $32 \times 32 \times 16$ mesh.

Figure 2. Normalized ion thermal fluxes in x as a function of time and wavenumber spectra in k_y for $k_x=0$ and k_z =fundamental averaged over the last third of the simulation for simulations with 6×10^5 particle ions and spatial smoothing given by (a) $\exp(-k^2 a^2)$, (b) $\exp(-k^4 a^4)$, and (c) $\exp(-k^6 a^6)$ with $a=1$.

Figure 3. Normalized ion thermal flux in x as a function of time for $V_0 \tau_S/c_s=0, 1, 2,$ and 4 in two-dimensional simulations.

Figure 4. Normalized ion thermal flux in x as a function of time for $V_0 \tau_T/c_s=0$ and 0.02 with no magnetic shear in two-dimensional simulations.

Figure 5. Normalized ion thermal flux in x and the effective potential energy (field + ion polarization + adiabatic electron kinetic energies) as functions of time for $V_0 \tau_S/c_s=0$ and 1 .

Figure 6. Normalized ion thermal flux in x and the effective potential energy as functions of time for $V_0 \tilde{L}_S/c_s=2$ and 3. Note the differences in vertical scales from those in Fig. 5.

Figure 7. The normalized ion thermal flux in x as a function time for $V_0 \tilde{L}_S/c_s$ switched from 0 to 3 half way through the simulation.

Figure 8. Normalized ion thermal flux in x as a function of time for $V_0 \tilde{\rho}_i \tilde{L}_S/c_s=1.8$ and -1.8 with $V_0 \tilde{\rho}_i=0$.

Figure 9. Normalized ion thermal fluxes in x as a function of time, profiles of $e\phi/T_e$ vs. x , and equi-potential contours of $e\phi/T_e$ vs. x and y after saturation for three-dimensional simulations including self-generated ion flows with externally imposed component of sheared $\mathbf{E} \times \mathbf{B}$ velocity given by (a) $V_0 \tilde{L}_S/c_s=0$ and (b) $V_0 \tilde{L}_S/c_s=2$.

Figure 10. Schematic of resonant intervals in the (x, v_{\parallel}) plane.

Figure 11. The ion energy diffusivity $\hat{\chi}_i$ and γ/k^2 normalized to gyro-reduced Bohm transport $c_s \rho_s^2/L_T$ observed in three-dimensional δf gyrokinetic simulations as functions of $V_0 \tilde{L}_S/c_s$ and $V_0 \tilde{\rho}_i \tilde{L}_S/c_s$.

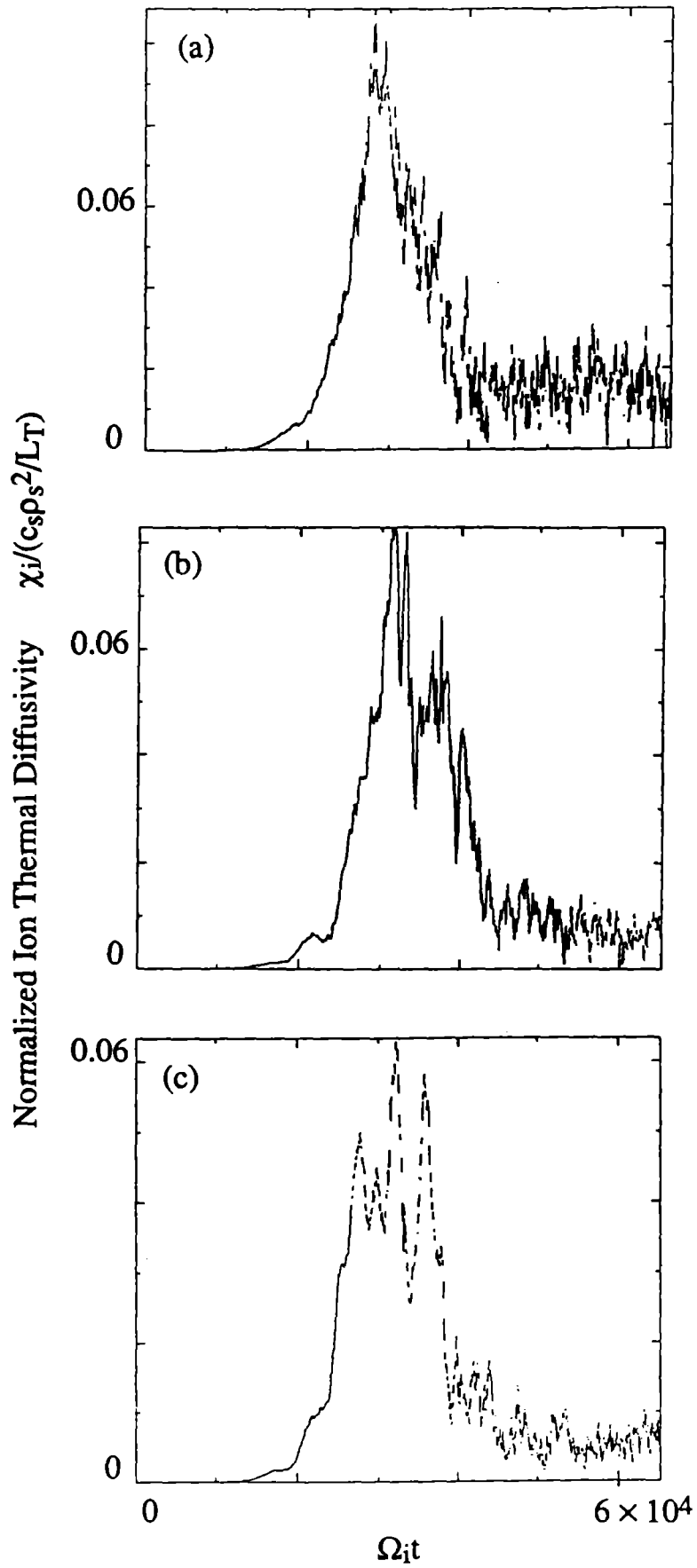


Figure 1

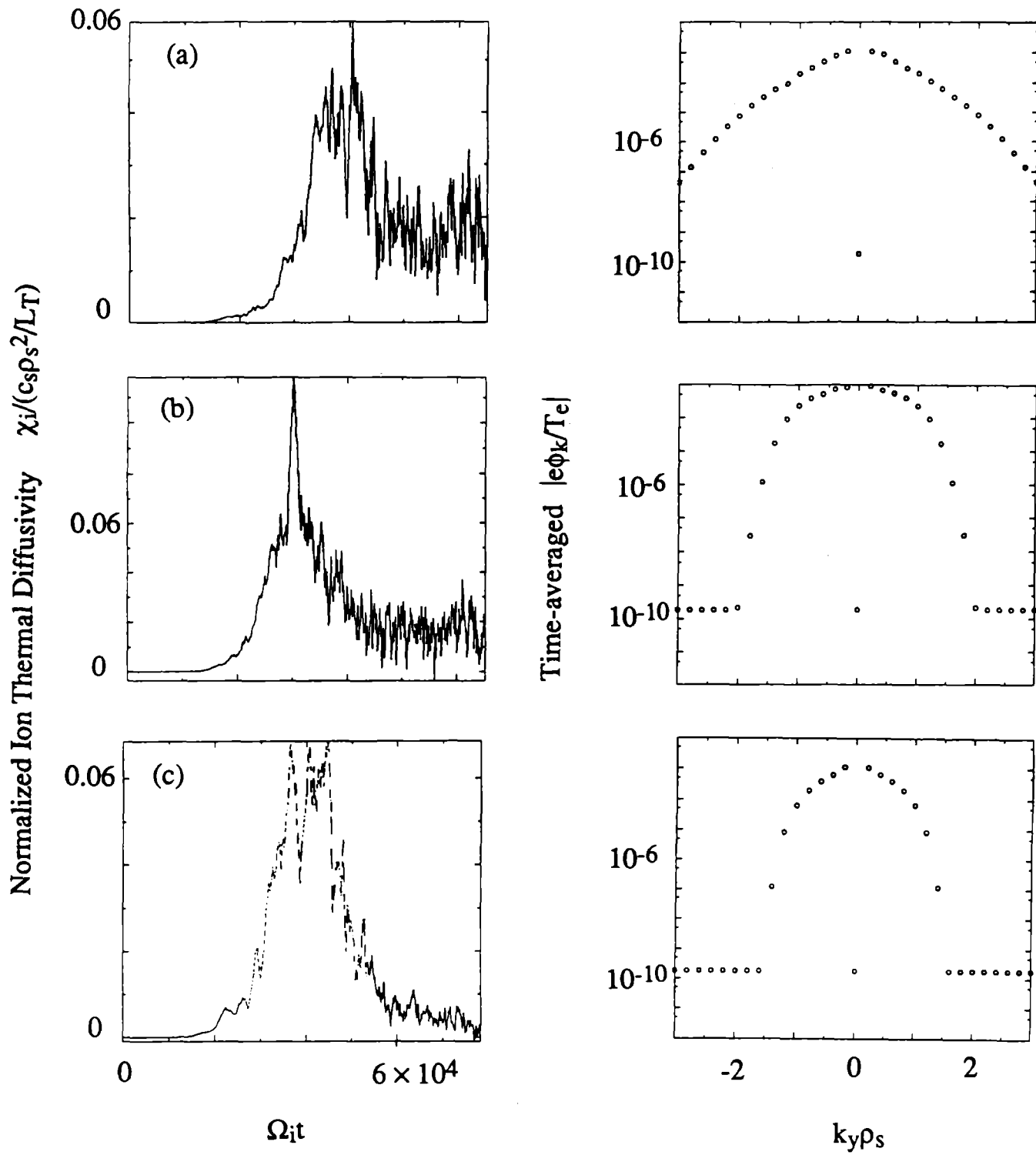


Figure 2

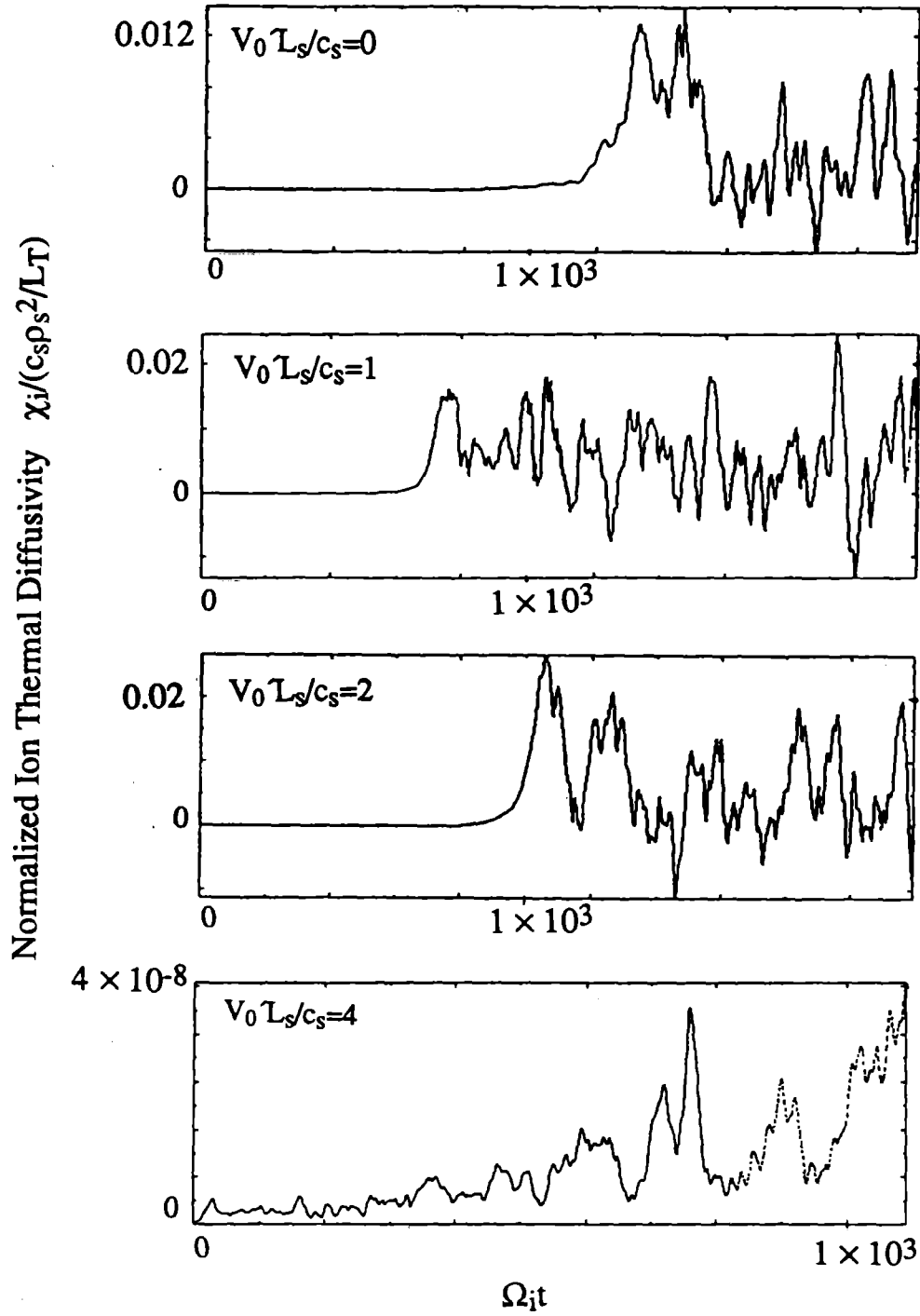


Figure 3

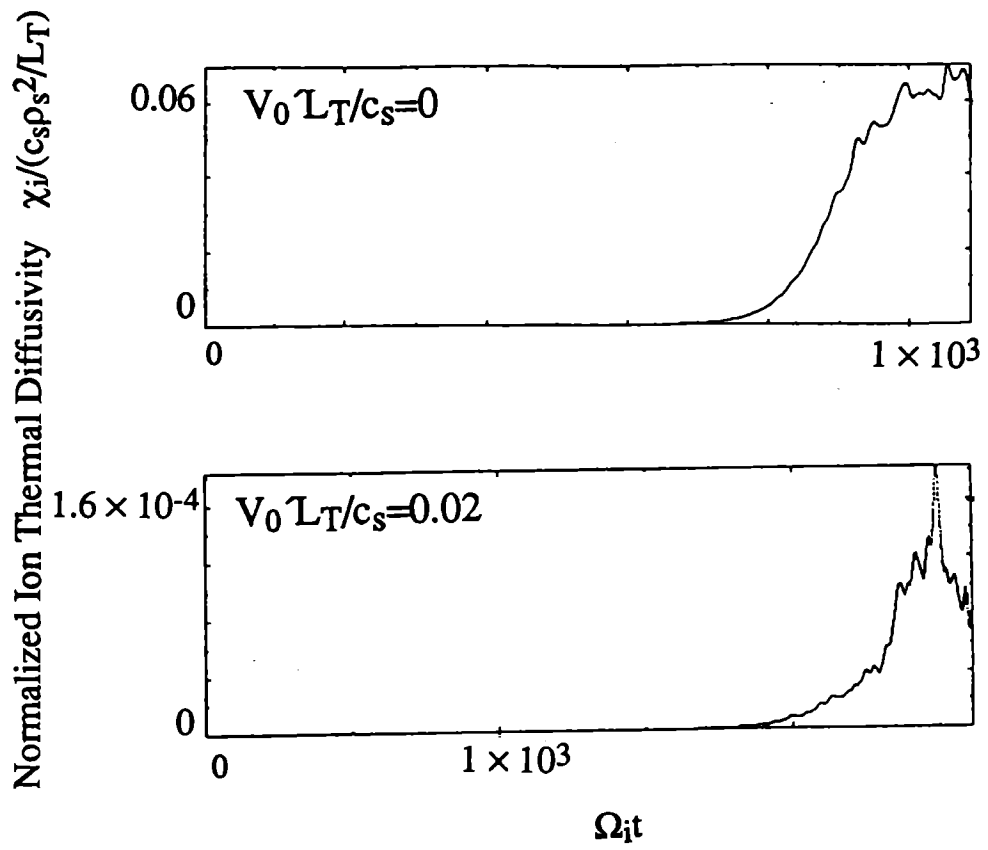


Figure 4

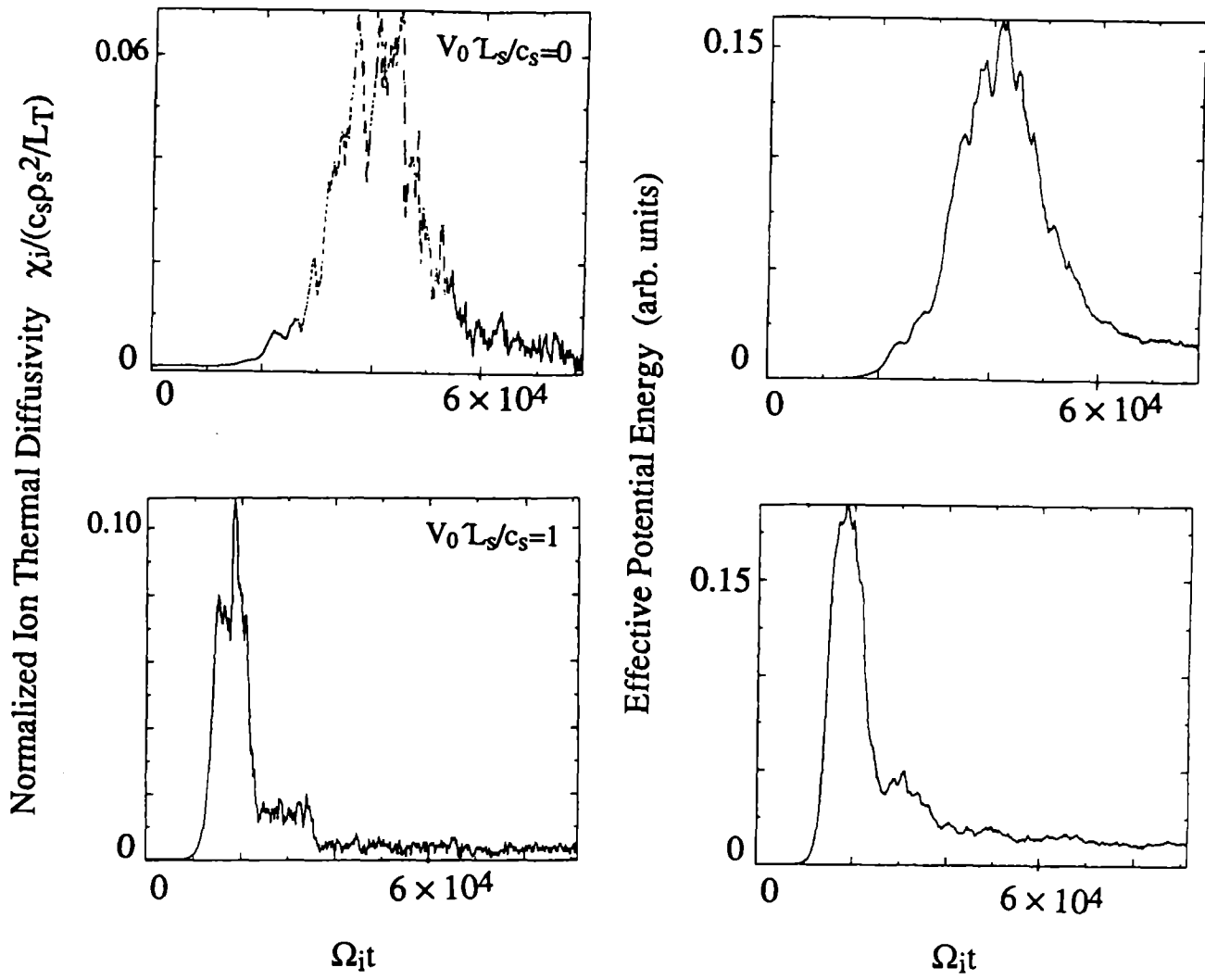


Figure 5

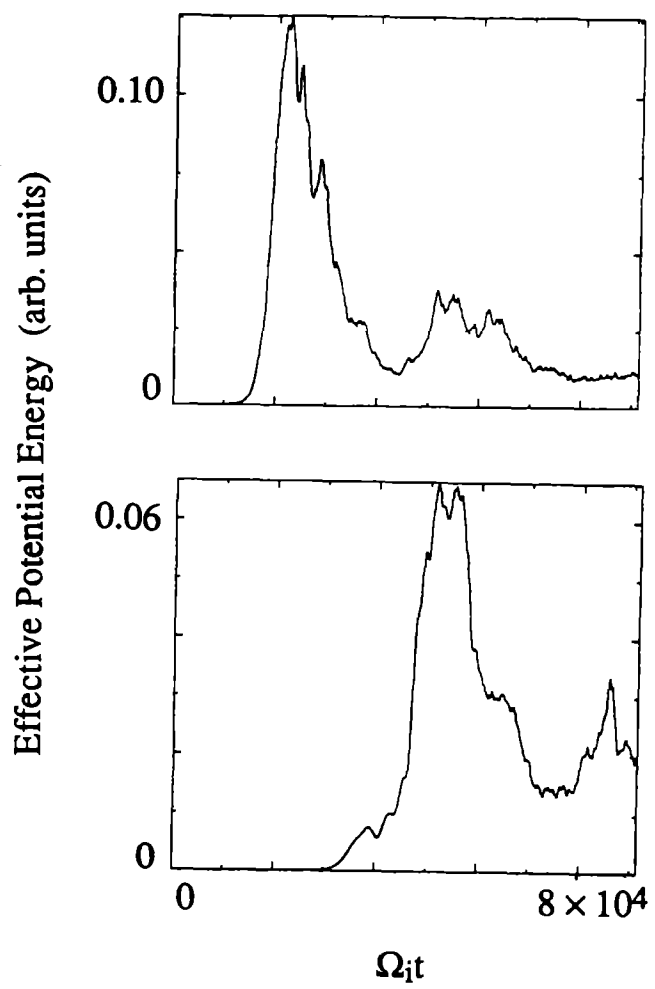
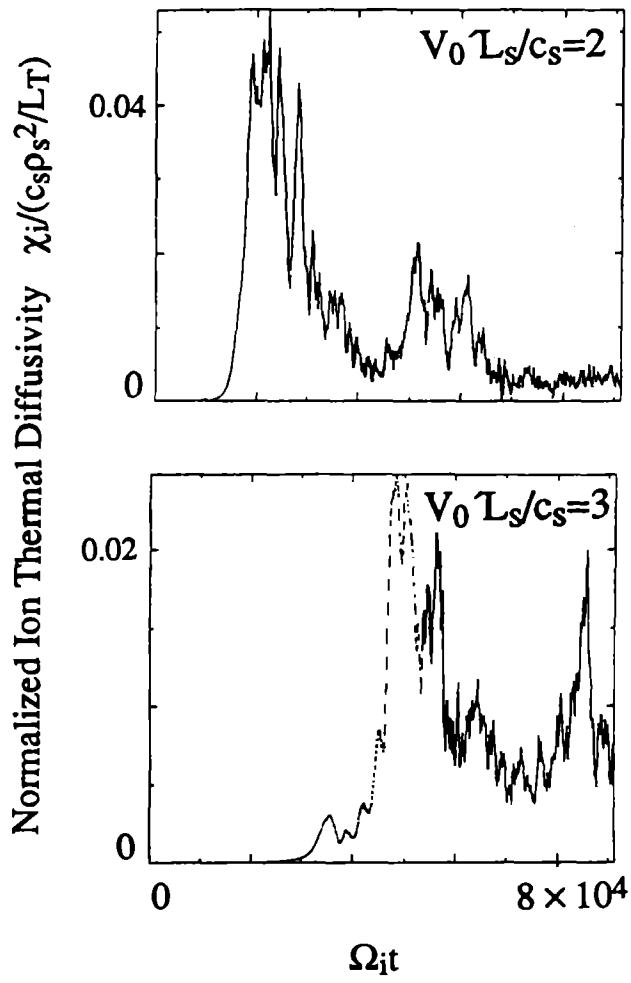


Figure 6

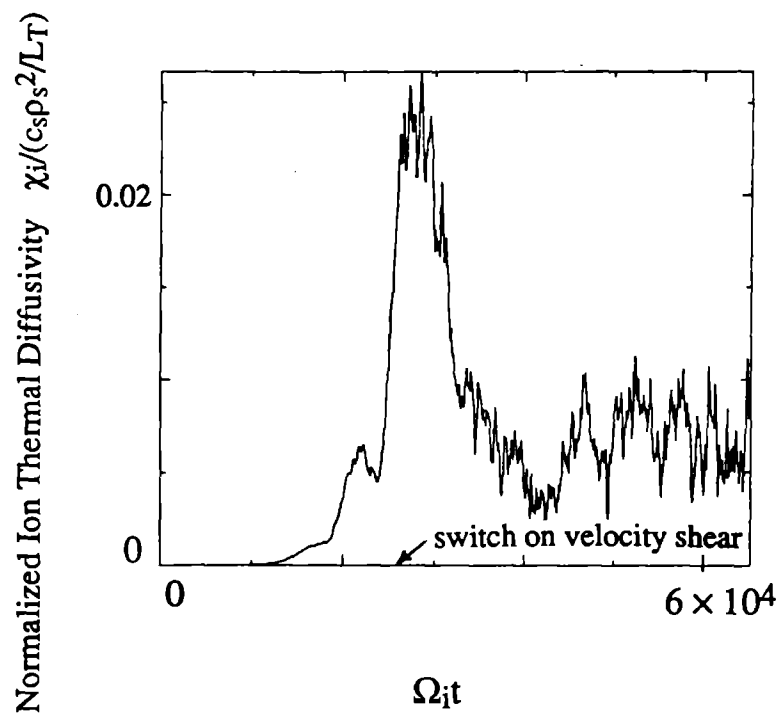


Figure 7

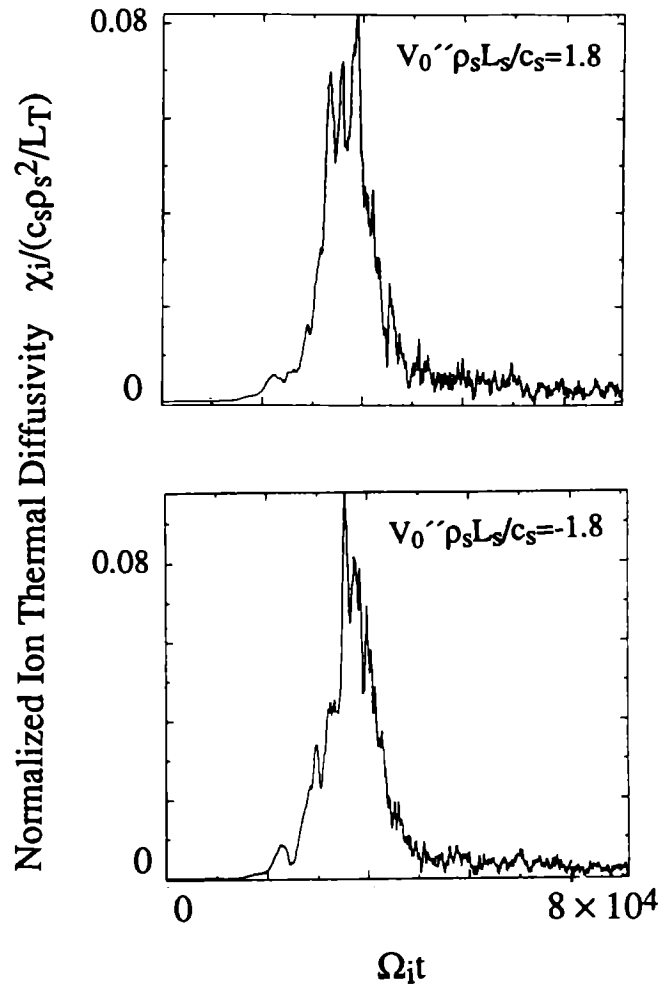


Figure 8

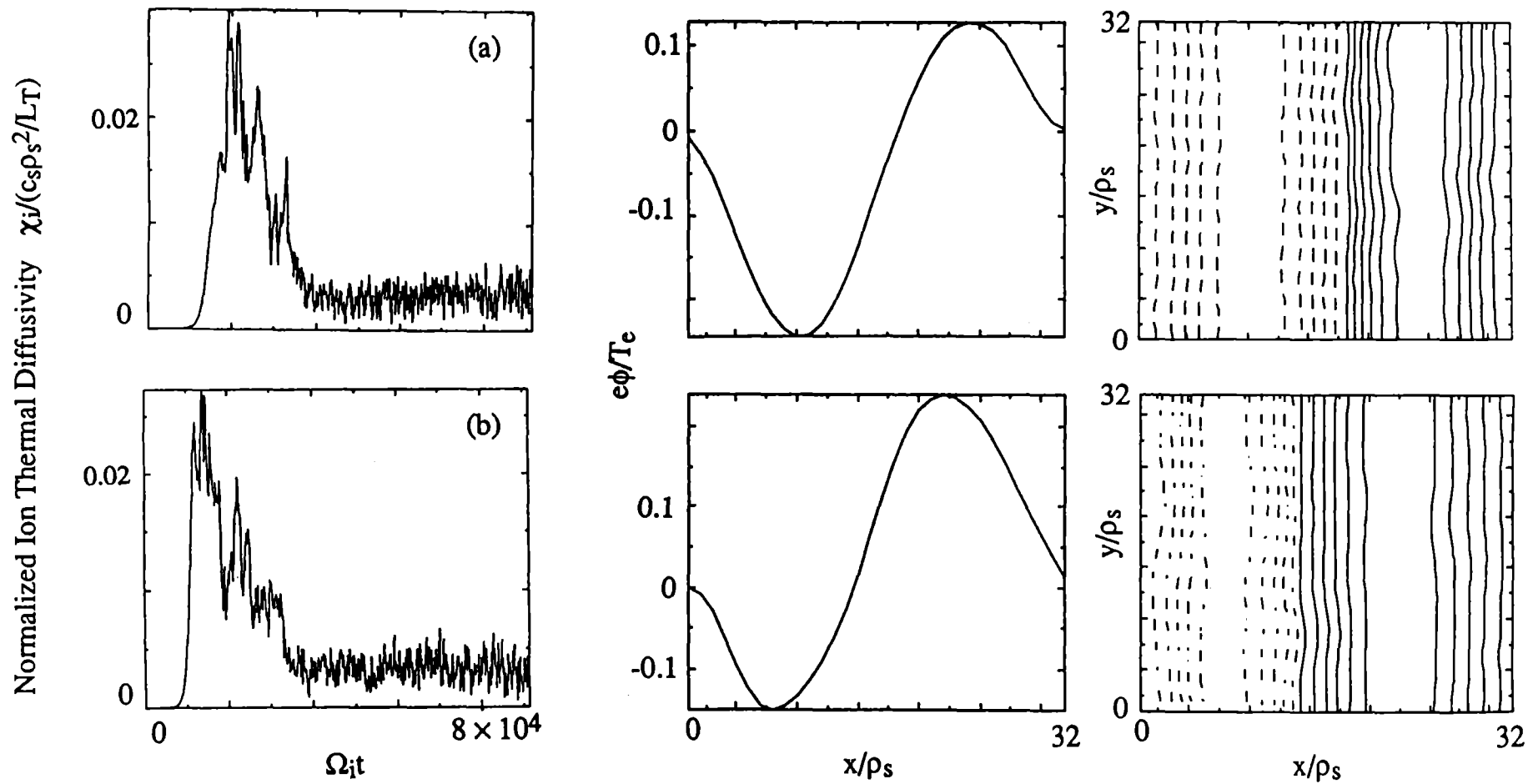


Figure 9

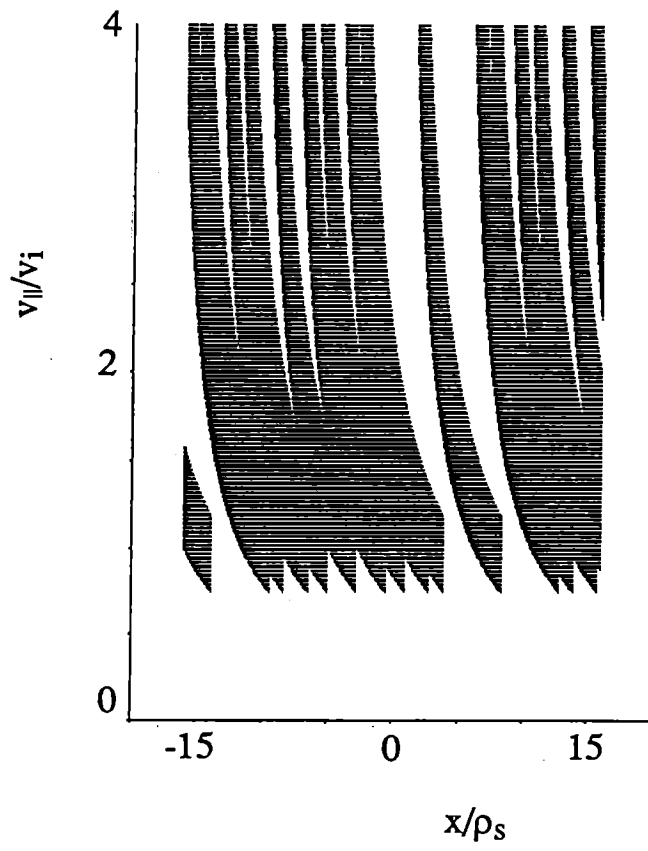


Figure 10

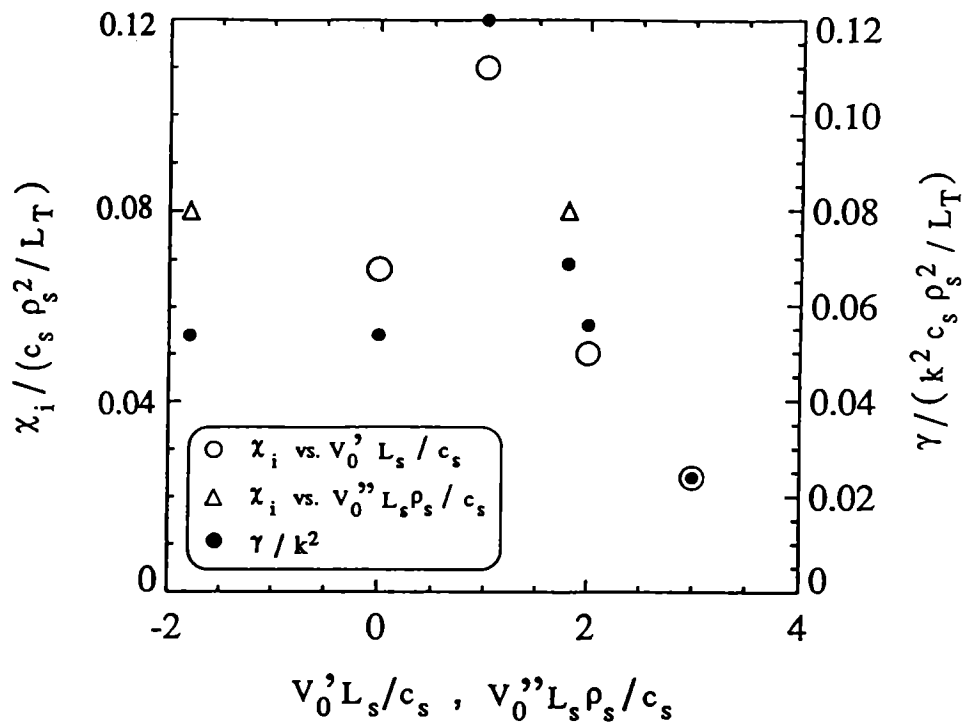


Figure 11

